Dynamic proportional-integral-differential controller for high-speed atomic force microscopy

Noriyuki Kodera and Mitsuru Sakashita
Department of Physics, Kanazawa University, Kakuma-machi, Kanazawa 920-1192, Japan

Toshio Ando
Department of Physics, Kanazawa University, Kakuma-machi, Kanazawa 920-1192, Japan
and CREST, JST, 4-1-8 Honcho Kawaguchi, Saitama 332-0012, Japan

(Received 4 April 2006; accepted 10 July 2006; published online 31 August 2006)

In tapping mode atomic force microscopy, the cantilever tip intermittently taps the sample as the tip scans over the surface. This mode is suitable for imaging fragile samples such as biological macromolecules, because vertical oscillation of the cantilever reduces lateral forces between the tip and sample. However, the tapping force (vertical force) is not necessarily weak enough for delicate samples, particularly for biomolecular systems containing weak inter- or intramolecular interactions. Light tapping requires an amplitude set point (i.e., a constant cantilever amplitude to be maintained during scanning) to be set very close to its free oscillation amplitude. However, this requirement does not reconcile with fast scans, because, with such a set point, the tip may easily be removed from the surface completely. This article presents two devices to overcome this difficulty; a new feedback controller (named as "dynamic proportional-integral-differential controller") and a compensator for drift in the cantilever-excitation efficiency. Together with other devices optimized for fast scan, these devices enable high-speed imaging of fragile samples. © *2006 American Institute of Physics.* [DOI: 10.1063/1.2336113]

I. INTRODUCTION

The atomic force microscope (AFM) has become an indispensable tool in imaging biological samples at high spatial resolutions (see reviews[1,2]). Amongst the various operating modes, tapping mode[3] has been most used when imaging biological samples in aqueous solutions because the oscillating cantilever tip exerts little lateral force on the sample. In order to gain the capability of tracing a protein in action at high temporal resolution with AFM, various efforts have recently been carried out.[4–11] The following devices and techniques have been developed, focusing mainly on enhancing the scan speed; small cantilevers[4–6,12] with a high resonant frequency and a small spring constant, an optical deflection detection system compatible with small cantilevers,[4–6] a fast rms-to-dc converter to quickly measure the oscillation amplitude of a cantilever,[4] a high-speed scanner with minimal structural resonance,[4,5] an active damping technique to eliminate resonant vibrations of the piezoactuators,[13] and a feedforward controller[14–16] capable of lightening the task of the feedback loop that maintains a constant tapping amplitude. A combination of some of these efforts has produced a high-speed AFM that can capture moving protein molecules on video at 80 ms/frame.[4,5,17,18] However, efforts to minimize the tapping force have not extensively been carried out. For example, forces involved in a highly dynamic protein-protein interaction are very weak. In order to image molecular processes that contain such weak interactions, the oscillating cantilever tip should barely come in contact with the sample.

First of all, the spring constant of small cantilevers has to be minimized to reduce the tapping force. However, it is almost determined by the balance with the resonant frequency required for fast imaging. Although a large quality factor Q can reduce the tapping force,[19,20] it slows the cantilever response, which is incompatible with fast imaging. Reduction of the cantilever's oscillation amplitude is one possibility but increases lateral forces between the tip and sample. In order for the oscillating cantilever tip to touch the sample surface with minimal force, the amplitude set point A_s (the peak-to-peak oscillation amplitude to be maintained during scanning) should be set very close to the free oscillation peak-to-peak amplitude $2A_0$. This too is incompatible with fast imaging because in this situation the cantilever tip tends to be detached completely from the sample surface, especially at steep downhill locations of the sample. Once detached, the tip will not quickly land again on the surface (parachuting), because of feedback saturation [the error signal is saturated at small values of $(2A_0-A_s)$, irrespective of how far the tip is separated from the surface at the end of its bottom swing]. At faster scan speeds, the parachuting effect would be increased. In addition, a small drift lowering the cantilever-excitation efficiency significantly affects the small difference, $(2A_0-A_s)$, which may make $2A_0$ less than A_s and consequently lead to complete detachment between the tip and sample. Thus, it is very difficult to make the fast scan and "light touching" compatible with each other. In this article we overcome this difficulty by developing a new feedback controller ["dynamic proportional-integral-differential (PID) controller"] and a compensator for drift in the cantilever-excitation efficiency. The dynamic PID controller can avoid feedback saturation and give much less dependence of the feedback bandwidth on A_s. The compensator

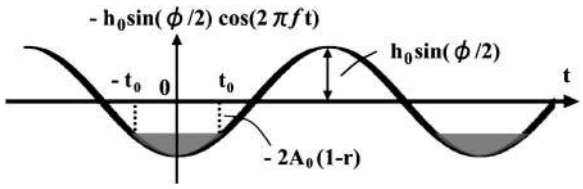

FIG. 1. The residual topography to be sensed by a cantilever tip under feedback control. When the maximum height of the residual topography is larger than the difference $(2A_0-A_s)$, the tip completely detaches from the surface. The untouched areas are shown in gray. The average tip-surface separation $\langle d\rangle$ at the end of cantilever's bottom swing is given by $\langle d\rangle = (1/2t_0)\int_{-t_0}^{t_0}[-2A_0(1-r)+h_0\sin(\phi/2)\cos(2\pi ft)]dt$, where $t_0=\beta/2\pi f$ (see the text). This integral results in $\langle d\rangle = 2A_0(1-r)[\tan\beta/\beta-1]$.

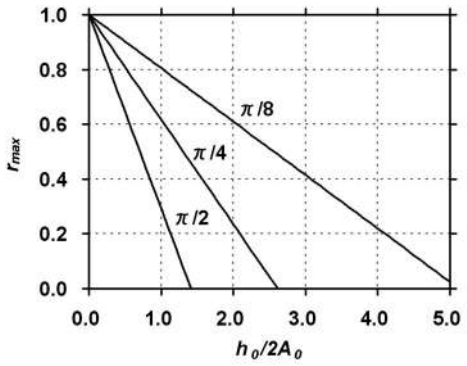

FIG. 2. The maximum amplitude set point $r_{\max}$ allowed for the cantilever tip to trace the sample surface without complete detachment from the surface, and its dependence on the ratio of the sample height h_0 to the free oscillation peak-to-peak amplitude $2A_0$ of the cantilever. The number attached to each line indicates the phase delay of the feedback operation.

stabilizes the cantilever's free oscillation amplitude. With the use of these controls together, high-speed and stable successive imaging becomes possible even for fragile samples which would either be destroyed or not be imaged quickly with a conventional PID controller. Brief descriptions of preliminary work on the dynamic PID control were previously presented.[17,18]

II. THEORETICAL CONSIDERATIONS

Here we analyze the dependence of feedback bandwidth on the set point A_s, the free oscillation amplitude A_0, the sample height h_0, and other factors. Similar analyses were previously presented by Sulchek *et al.* in a qualitative manner[10] and by us in a semiquantitative manner.[21] Here, we present analytical expressions. Suppose that a sample on a substrate has a periodicity of λ and that the sample stage is moved horizontally with a velocity V_s, the spatial frequency $1/\lambda$ is converted to a temporal frequency $f=V_s/\lambda$. This is the feedback frequency at which the sample stage is moved in the z direction. When the phase of the feedback signal is delayed by ϕ, a cantilever tip senses the "residual sample topography" $\Delta S(t)$ as a function of time (see Fig. 1). $\Delta S(t)$ is expressed as

$$\Delta S(t) = \frac{h_0}{2}[\sin(2\pi ft) - \sin(2\pi ft - \phi)] = h_0 \sin\frac{\phi}{2}\cos\left(2\pi ft - \frac{\phi}{2}\right), \quad (1)$$

where h_0 is the maximum height of the sample. The maximum height of the residual topography $h_0\sin(\phi/2)$ should be smaller than $(2A_0-A_s)$, otherwise the cantilever tip would occasionally detach itself completely from the sample surface. This condition restricts the maximum value of $r \equiv A_s/2A_0$ according to Eq. (2) given below, as a function of $h_0/2A_0$ and ϕ (see Fig. 2),

$$r < 1 - \frac{h_0}{2A_0}\sin\frac{\phi}{2}. \quad (2)$$

The phase delay ϕ is given by $2\pi f\Delta\tau$, where $\Delta\tau$ is the time delay of the feedback control. The time delay is caused by various factors; the main delays are in the time of reading the cantilever's oscillation amplitude (it takes at least $1/2f_c$), the cantilever's response time $(Q_c/\pi f_c)$, and the z-scanner's response time $(Q_s/\pi f_s)$, where Q_c and f_c are the quality factor and resonant frequency of the cantilever and Q_s and f_s are the quality factor and resonant frequency of the z scanner, respectively. These delays and other delays (the total δ) give the following relationship:

$$f = \frac{\phi f_c}{2\pi}\Bigg/\left(\frac{1}{2} + \frac{Q_c}{\pi} + \frac{Q_s f_c}{\pi f_s} + f_c\delta\right). \quad (3)$$

Here, we have to note that the delays can be compensated for to some extent by a differential operation with the PID feedback controller. When the cantilever tip is completely detached from the sample surface at the end of its bottom swing, it takes a time to touch the surface again. This adds an additional delay $\Delta\tau_d$. For the first approximation, Eq. (1) is assumed to hold even in this case. The average separation during detachment is given by $2A_0(1-r)[(\tan\beta)/\beta-1]$, where β is $\cos^{-1}[2A_0(1-r)/h_0\sin(\phi/2)]$ (see Fig. 1). The feedback gain is usually set to a level at which the separation distance of $2A_0(1-r)$ diminishes roughly in a single period of the cantilever oscillation. Therefore, the additional time delay $\Delta\tau_d$ is roughly given by $[(\tan\beta)/\beta-1]/f_c$. By introducing this additional delay into Eq. (3), we can obtain the feedback bandwidth as a function of various parameters [Eq. (4) and Fig. 3, where the phase delay is set at $\pi/4$],

$$f = \frac{f_c}{8}\Bigg/\left(\frac{Q_c}{\pi} + \frac{Q_s f_c}{\pi f_s} + f_c\delta + \frac{\tan\beta}{\beta} - \frac{1}{2}\right). \quad (4)$$

When r is smaller than $[1-(h_0/2A_0)\sin(\pi/8)]$, β becomes zero and thus the feedback bandwidth is independent of r. As seen in Fig. 3, the feedback bandwidth decreases with increasing r and rapidly approaches zero at $r>0.9$.

III. MATERIALS AND METHODS

A. High-speed AFM apparatus

A high-speed atomic force microscope developed in our laboratory and nearly the same as that described previously[4,5] was used. The z-piezoactuators were replaced with those having a higher resonance frequency of 400 kHz (custom made, NEC-Tokin, Japan). In addition, vibrations of the z-piezoactuators are actively damped using an active damping technique,[13] resulting in no resonant vibrations. The bandwidth of this z scanner is about 150 kHz. The PID feed-

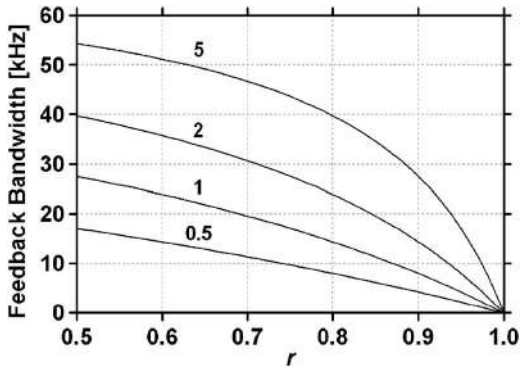

FIG. 3. Theoretically derived feedback bandwidth as a function of the ratio r of the amplitude set point to the free oscillation peak-to-peak amplitude of the cantilever. The number attached to each curve indicates the ratio $2A_0/h_0$. The feedback bandwidths were obtained under the following conditions: the cantilever's resonant frequency, 1.2 MHz; quality factor of the cantilever oscillation, 3; the resonant frequency of the z scanner, 150 kHz; and quality factor of the z scanner, 0.5.

back circuit was replaced with the dynamic PID controller whose design and characteristics are presented in this article. However, which of these two controllers is active can be selected by a switch. Small cantilevers used here were supplied by Olympus.[12] They have a resonant frequency of ~1.2 MHz in water and a spring constant of ~200 pN/nm. The tips are grown by electron-beam deposition. The tip length was adjusted to approximately 1.0 μm. The second harmonic amplitude of the oscillating cantilevers was detected by using a lock-in amplifier (SR844-RF, Stanford Research Systems, Sunnyvale).

B. Mock AFM circuit

To execute quick and precise tests of the feedback loop performance, we developed a mock AFM circuit (Fig. 4). This circuit consists of two sets of second-order low-pass filters and a threshold circuit that can simulate a decrease in the cantilever's oscillation amplitude caused by tip-sample interaction. One of the low-pass filters has resonant properties (and hence a transfer function) very similar to those of the z scanner (resonant frequency: 150 kHz, Q: 18), and the other low-pass filter has resonant properties very similar to those of the small cantilevers (resonant frequency: ~1.2 MHz, Q: 2–3). In addition, the mock sample topography is produced by a wave-function generator. The mock z scanner is actively damped with a controller.[13]

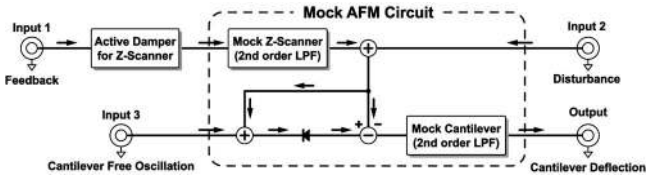

FIG. 4. Circuit diagram of a mock AFM system. Disturbance signals fed into the input 2 simulate sample topography. The output simulates the oscillation of a cantilever tip interacting with a sample surface. The amplitude change caused by the interaction is given by the diode.

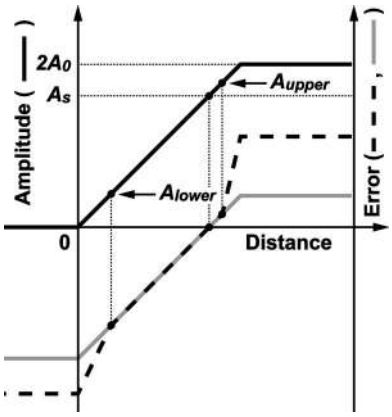

FIG. 5. Schematic showing the principle of the dynamic PID control. Solid line: an amplitude-distance curve; gray line: an error signal used in the conventional PID control; and broken line: an error signal used in the dynamic PID control.

C. Sample preparation and imaging

Myosin V was extracted from chick brains and purified as previously described.[22] Myosin V was stored at 0 °C in buffer A [25 mM KCl, 25 mM imidazole (pH 7.6), 2 mM $MgCl_2$, 1 mM ethylene glycol tetraacetic acid (EGTA), and 2 mM dithiothreitol]. Actin was prepared from rabbit skeletal muscles as previously described.[23] The purified actin (~50 μM) was stored as F-actin in buffer B [100 mM KCl, 2 mM $MgCl_2$, 0.2 mM $CaCl_2$, tris-HCl (pH 8.0), and 0.2 mM adenosine triphoshate (ATP)] on ice. Just before use, an aliquot of the F-actin solution was centrifuged (150 000 g, 1 h) to remove ATP and unpolymerized actin, and the pellet was suspended in buffer C [100 mM KCl, 2 mM $MgCl_2$, 1 mM EGTA, 0.1 mM NaN_3, and 25 mM imidazole (pH 7.6)]. For imaging myosin V attached to actin filaments, a few nanomolar myosin V was mixed with actin filaments (2 μM) in buffer C. One drop (~1.5 μl) of the sample was placed on freshly cleaved mica (1 mm ϕ) for 3 min, rinsed with buffer C, and imaged in buffer C.

IV. RESULTS

A. Dynamic PID feedback controller

With a conventional PID feedback circuit, the gain parameters cannot be automatically altered during scanning based on the topographic features of the sample. When an oscillating cantilever tip is completely detached from the sample surface, the error signal becomes saturated at $(2A_0 - A_s)$ (Fig. 5). When A_s is very close to $2A_0$, the saturated error signal is very small, and thus the detached tip will not quickly land again on the surface (parachuting). The PID gains could be increased to shorten the parachuting period. However, this increase promotes overshooting at uphill regions of the sample, especially near the peak of a local maximum on the sample, and consequently introduces instability in the feedback operation. This problem can be solved if the PID gains are regulated based on the cantilever's peak-to-peak oscillation amplitude $A_{p\text{-}p}$ relative to A_s. We devised such a feedback controller (dynamic PID controller) by inserting a circuit (termed "dynamic operator") between the error signal output and the input of a conventional PID cir-

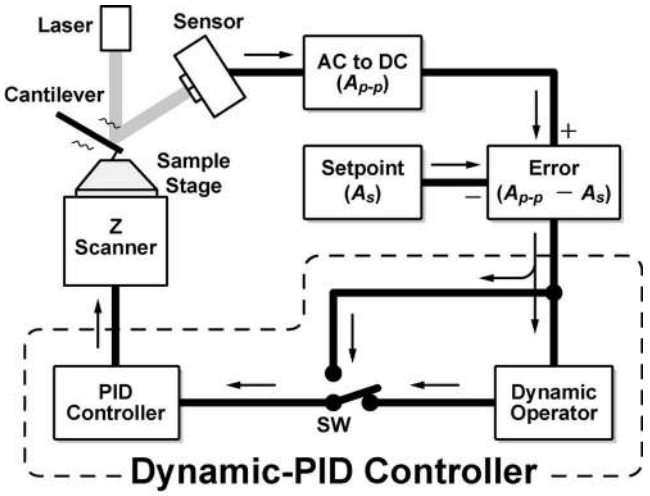

FIG. 6. Diagram of feedback loop with dynamic PID operator.

cuit (Fig. 6). This dynamic operator functions as follows (see Fig. 5). A threshold level A_{upper} is set between A_s and $2A_0$. When the cantilever's peak-to-peak oscillation amplitude $A_{\text{p-p}}$ exceeds A_{upper}, the differential signal $(A_{\text{p-p}}-A_{\text{upper}})$ is amplified and added to the error signal. The error signal that contains an extra signal is fed to the conventional PID. The "false error signal" which is larger than the "true error signal" produces a quicker feedback response, and therefore $A_{\text{p-p}}$ quickly becomes smaller than A_{upper} and the feedback operation automatically returns to the normal mode. Thus, even with A_s very close to $2A_0$, the parachuting period is shortened drastically, and hence no feedback saturation occurs. A similar manipulation of the error signal can be made as well when $A_{\text{p-p}}$ is smaller than A_s. In this case a new threshold level A_{lower} is set lower than A_s to an appropriate extent. When $A_{\text{p-p}}$ becomes lower than A_{lower}, the differential signal $(A_{\text{p-p}}-A_{\text{lower}})$ is amplified and then added to the error signal $(A_{\text{p-p}}-A_s)$. This manipulation can keep the cantilever tip from pushing into the sample too strongly, especially at steep uphill regions of the sample.

These manipulative operations are implemented by a circuit shown in Fig. 7. The circuit has three branches in the horizontal direction. The true error signal passes through the middle branch. A dc signal corresponding to $(A_{\text{upper}}-A_s)$ is

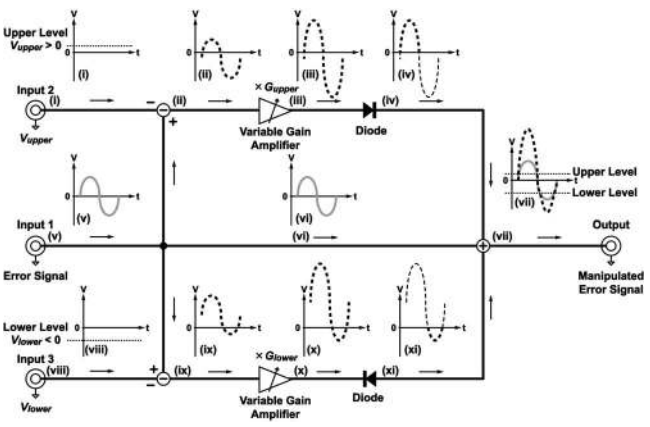

FIG. 7. Circuit diagram of dynamic operator. For details, see the text.

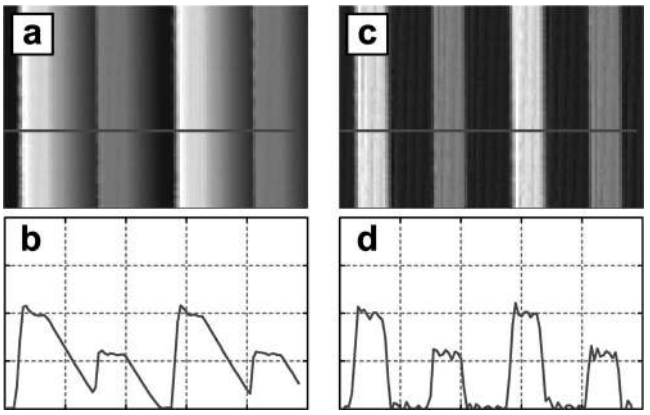

FIG. 8. Pseudo-AFM images of a sample with rectangles with two different heights. The images were obtained using a conventional PID controller (a) or using the dynamic PID controller (c). Lower panels (b) and (d) show line profiles of images (a) and (c), respectively. These simulations with the mock AFM system were made under the same condition shown in Fig. 3 captions. The line scan speed: 1 mm/s; the line scan frequency: 1 kHz; and the frame rate: 100 ms/frame.

fed to the upper branch input terminal and passes though a subtracter to produce $(A_{\text{p-p}}-A_{\text{upper}})$. The output is amplified (gain, G_{upper}), passed through a precision diode circuit, and finally summed with the true error signal. The precision diode circuit compensates for an offset inherent in the diode chip. The final output, $L[A_{\text{p-p}}-A_{\text{upper}}]\times G_{\text{upper}}+(A_{\text{p-p}}-A_s)$, is fed to the conventional PID input terminal. Here, L is the operator that acts as $L[x]=x$ (if $x>0$) or $L[x]=0$ (if $x\leqslant 0$). The signal $(A_{\text{p-p}}-A_{\text{upper}})$ could be constructed directly from $A_{\text{p-p}}$ and A_{upper}. However, in this case, A_{upper} has to be tuned depending on A_s, because A_{upper} has to be larger than A_s. On the other hand, using the method we employed above, the positive dc signal, corresponding to $(A_{\text{upper}}-A_s)$, is tuned independently from A_s. The false error signal, $-L[A_{\text{lower}}-A_{\text{p-p}}]\times G_{\text{lower}}+(A_{\text{p-p}}-A_s)$, is similarly constructed for the lower branch.

B. Performance test of dynamic PID using a mock AFM

Feedback performance of the dynamic PID controller was compared with that of a conventional PID controller using a mock AFM. Herein, a mock cantilever with $Q=3$ oscillating at its resonant frequency of 1.2 MHz is scanned over a mock sample surface (rectangular shapes with two different heights) from left to right at scan speed of 1 mm/s (frame rate of 100 ms/frame). Here, $2A_0$ is the same as the taller sample height, and A_s is set at $0.9\times 2A_0$. With the conventional PID controller, the topographic image became blunt [Fig. 8(a)]. As seen in the line profile [Fig. 8(b)], parachuting occurred significantly at steep downhill regions. On the other hand, use of the dynamic PID controller produces a clear image [Fig. 8(c)] and almost no parachuting occurred [Fig. 8(d)].

Next, we examined performance of the dynamic PID by measuring feedback bandwidth as a function of $h_0/2A_0$ and $r(=A_s/2A_0)$, using the mock AFM, and compared it with that of the conventional PID. Here, we did not use the dynamic operator of the lower branch (i.e, $G_{\text{lower}}=0$, see Fig. 7). The

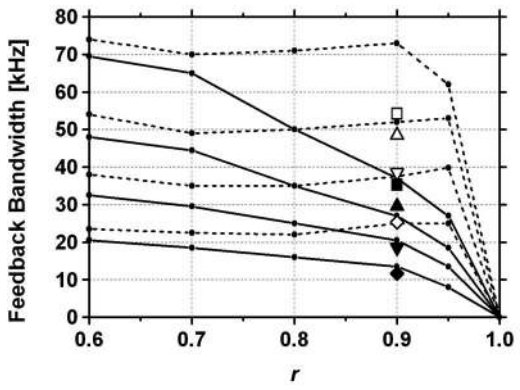

FIG. 9. Feedback bandwidth as a function of the ratio $r=A_s/2A_0$, measured using the mock AFM system or the real AFM system. Solid-line curves: feedback bandwidths measured using the mock AFM system with a conventional PID controller; dotted-line curves: feedback bandwidths measured using the mock AFM system with the dynamic PID controller; closed marks: feedback bandwidths with $2A_0/h_0=0.5$(♦), 1(▼), 2(▲), and 5(■) measured using the real AFM system with the conventional PID controller; and open marks: feedback bandwidths with $2A_0/h_0=0.5$(◇), 1(▽), 2(△), and 5(□) measured using the real AFM system with the dynamic PID controller. The solid-line curves and the dotted-line curves are aligned from top to bottom according to the ratio $2A_0/h_0=5$, 2, 1, and 0.5.

feedback bandwidth was determined as a frequency of disturbance signals (sinusoidal waves that simulate sample topography) that gave 45° phase delay to the feedback controller output. Although the disturbance should be applied to the mock cantilever, it was applied to the mock z scanner for a reason mentioned in the next section. First, the gain parameters of the conventional PID controller were adjusted to provide the best performance (a minimal error signal rms) for each r and for $h_0/2A_0=1$. The gain parameters were not altered for various ratios of $h_0/2A_0$. After measuring various bandwidths, the gain parameters of the dynamic PID controller were adjusted (the P, I, and D gains were slightly attenuated) for the same r, and then the gain parameter (G_{upper}, see Fig. 7) of the dynamic operator was adjusted. The threshold level A_{upper} was set to be slightly higher than A_s. The adjustment of the PID gains and G_{upper} was performed so as to produce no shift of the dc level of the mock cantilever deflection from A_s and a minimal rms value of the true error signals. The results of these measurements are summarized in Fig. 9. The maximum feedback bandwidth obtained was about 70 kHz, which was higher than the frequency expected from Eq. (3) with $\delta=0$ (about 55 kHz), due to a compensation effect by the D operator of the PID feedback control. With the conventional PID control, feedback bandwidth decreased with increasing r and $h_0/2A_0$. These behaviors were very similar to the results obtained from theoretical analysis (Fig. 3). On the other hand, feedback bandwidth was nearly even over the set point range examined ($0.6<r<0.95$) using the dynamic PID control. In addition, the maximum feedback bandwidth observed at each $h_0/2A_0$ was always higher than the corresponding bandwidth obtained with the conventional PID control. When A_{upper} was varied between A_s and $2A_0$, the resulting feedback bandwidth did not change as long as optimum adjustment of G_{upper} and the PID gain parameters was made.

C. Performance test of dynamic PID using a high-speed AFM

We examined whether the excellent performance of dynamic PID witnessed during testing using the mock AFM was also true with a real AFM system. In this examination, A_0 and A_s were fixed at 5.5 nm and $0.9\times 2A_0$ (9.9 nm), respectively, to measure feedback bandwidth. Because it was difficult to prepare test samples with sinusoidal wave topographies, mica (immersed in water) on the sample stage was moved in the z direction at various frequencies and with various amplitudes. This is the reason why in the aforementioned experiment, perturbation was applied to the mock z scanner. A sinusoidal signal for moving the sample stage was added to the output of the conventional PID circuit or the dynamic PID circuit and their sum was fed into a z-piezoactuator driving amplifier. As indicated in Fig. 9, the feedback bandwidths obtained here were very similar to the corresponding values obtained using the mock AFM, except for the case $2A_0/h_0=5$. The disagreement observed with $2A_0/h_0=5$ arises from a relatively low signal to noise ratio of the sensor signal when the z scanner is perturbed by sinusoidal waves with a small amplitude ($h_0=2.2$ nm). The gain parameters of the dynamic PID controller could not be increased much due to the sensor noise.

We have to note that the feedback bandwidth measured using the mock or real AFM systems is underestimated, because the perturbation was applied to the (mock) z scanner. When the perturbation was applied to the mock cantilever (which is more close to the actual situation in imaging), the observed feedback bandwidths were always 30%–40% higher than the corresponding values given in Fig. 9. This is due to the slower response speed of the (mock) z scanner, compared with the small cantilevers.

D. Drift compensation

Compared with contact mode imaging, tapping mode imaging is not significantly affected by drifts in various components of AFM. This is because in tapping mode, the tip-sample interaction is reflected only on the ac component of the signal from the cantilever-deflection detector and thus drift in its dc component hardly affects the imaging performance. Drifts, however, are still problematic even in tapping mode imaging. Some efforts to compensate for drifts in the deflection sensor signal were previously carried out. Kindt *et al.*[24] controlled the deflection set point or amplitude set point using a cross correlation of the feature richness between two traces (forward and backward traces) at slightly different set points. Although this method works well for both contact and tapping modes, calculations for the cross correlation must be made for every line scan, and therefore additional efforts are required to make it compatible with fast imaging. In tapping mode, drift in the cantilever-excitation efficiency is the most problematic one, particularly when A_s is set very close to $2A_0$ to minimize the tapping force. The AFM apparatus misunderstands this drift-caused change in the cantilever oscillation amplitude and interprets the change as a result of tip-sample interaction. For example, when the excitation efficiency is lowered, the AFM apparatus interprets this as

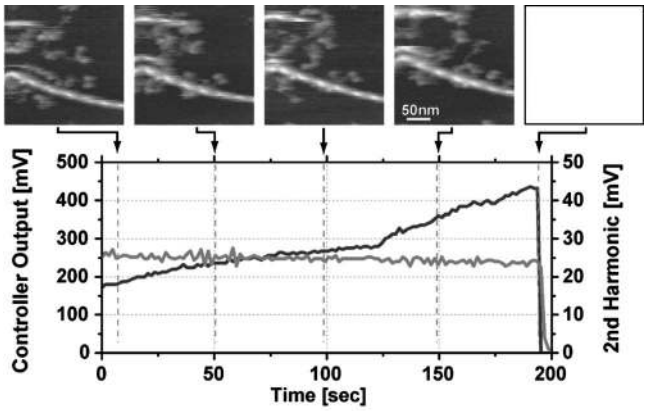

FIG. 10. Successive imaging of myosin V attached to actin filaments using a compensator for drift in the cantilever-excitation efficiency. The imaging was successively made for 3 min at frame rate of 10 frames/s and with $A_0=2.5$ nm and $r(A_s/2A_0)=0.92$. Only five images obtained at times indicated by arrows are shown. Black line: the output from the drift compensator; gray line: the second harmonic amplitude. At 3 min, the compensator was switched off.

the tip interacting with the sample too strongly. Therefore, the feedback responds by withdrawing the sample stage from the tip, which is an incorrect direction. Without stability in the excitation efficiency or A_0, successive imaging under a small tapping force cannot be realized. The drift may be caused by an increase in the temperature of the oscillating piezoactuator ("excitation actuator" for driving cantilever oscillation), by a change in an area of the fluid cell in contact with a buffer solution, and by a change in the cantilever resonance frequency. It is difficult to eliminate these causes. In addition, we cannot detect the free amplitude A_0 while imaging. This problem was previously challenged by Schiener *et al.*[25] They used the second harmonic amplitude of cantilever oscillation to detect drifts. The second harmonic amplitude is sensitive to tip-sample interaction, and therefore, drift in A_0 is reflected in the amplitude averaged over a period longer than the image-acquisition time. Instead of controlling A_0, they controlled A_s in order to maintain the constant difference $(2A_0-A_s)$. However, this control varies the tapping force and feedback bandwidth because $h_0/2A_0$ changes. To compensate for drift in the cantilever-excitation efficiency here, we also used the second harmonic amplitude of cantilever oscillation, but instead of controlling A_s we controlled the output gain of a wave generator (WF-1946A, NF Corp., Osaka, Japan) connected to the excitation piezoactuator. We used only a type I controller whose time constant was adjusted to 1–2 s (about ten times longer than the image-acquisition time). The performance of this drift compensation is shown in Fig. 10. A sample of myosin V bound to actin filaments in solution was imaged successively for 3 min at 100 ms/frame. Very stable imaging was achieved, even with the small difference $(2A_0-A_s)=0.4$ nm. In addition, the fragile actin filaments were never disassembled during imaging. The output signal from the type I controller was increasing with time, indicating that the cantilever-excitation efficiency was declining with time. On the other hand, the second harmonic amplitude was kept constant. When the the type I controller output was disconnected after 3 min, no image was obtained because of complete detachment between the tip and sample.

V. DISCUSSION

Feedback bandwidth is the most important factor in high-speed AFM imaging. In tapping mode, feedback bandwidth (defined by 45° phase delay) cannot exceed one-fourth of the cantilever's resonant frequency [see Eq. (4)]. This is because at least a half period of the cantilever oscillation is required for reading its amplitude. In addition, the cantilever's Q factor slows its response to the tip-sample interaction and hence lowers the feedback bandwidth. Thus, high-speed tapping mode AFM requires cantilevers having a small Q and a high resonant frequency that is at least five to six times greater than the required feedback bandwidth. However, there is a practical limit in reconciling the high resonance frequency with a small spring constant. Accordingly, fast imaging is difficult to achieve under a nondestructive imaging condition.

One of the main purposes of fast imaging of biological samples is to observe their dynamic behaviors as they function in solution. Hence, minimization of the tip-sample interaction force is essential. It requires a wide feedback bandwidth as well as a small tapping force. In a conventional PID circuit, gains are the same for both regimes of $A_{\text{p-p}}>A_s$ and $A_{\text{p-p}}<A_s$. In order to shorten the parachuting period (where $A_{\text{p-p}}>A_s$), the gains must be large. However, to avoid overshoots at uphill regions of the sample (where $A_{\text{p-p}}<A_s$), the gains have to be attenuated. Thus, the gains have to be determined via a balance between these two aspects. In the dynamic PID control, appropriate gains are separately adjusted for the two regimes. This is the key for its excellent performance. The dynamic PID control improves both feedback bandwidth and tapping force simultaneously and will therefore become indispensable in high-speed AFM imaging of delicate samples.

Its implementation can be made with a simple analog circuit (the dynamic operator and a conventional PID controller) and should be able to be implemented in a digital signal processor system. We inserted the dynamic operator between the error signal output and the input to a conventional PID controller. However, there may be some variations. For example, the outputs from the upper and lower branches (see Fig. 7) can be added directly to the conventional PID controller output. A similar function can be obtained with a different design; a voltage-controlled variable gain amplifier is placed on each output of the two PI or three PID components, where the error signal is used for controlling the gains. Better performance may be obtained using one of these methods or possibly other variations.

The dynamic PID control for regime $A_{\text{p-p}}<A_s$ is not as effective as it is for regime $A_{\text{p-p}}>A_s$, particularly when A_s is set very close to A_0, because in the regime $A_{\text{p-p}}<A_s$ the error signal hardly saturates. In addition, this control for the regime $A_{\text{p-p}}<A_s$ may produce ill effects on the feedback operation when the threshold level A_{lower} is set close to A_s. It promotes overshoot of the cantilever tip and hence induces its parachuting. However, this control is still useful when the

threshold level A_{lower} is set far from A_s and is close to zero. It can avoid tip-sample contact that is too strong and thus prevents damage of both the sample and tip. A similar control system for avoiding overly strong tip-sample contact can be constructed and used for the preimaging operation of the sample stage approaching the cantilever tip.

Compared with the first generation of high-speed AFM,[4,5] faster, more stable, and nondestructive imaging has become possible, owing to the dynamic PID controller and the drift compensator developed here. From this ability and improvements that will come forth, high-speed AFM is anticipated to play an active role in biological sciences in the near future.

ACKNOWLEDGMENTS

This work was supported by CREST/JST, Special Coordination Funds for Promoting Science and Technology (Effective Promotion of Joint Research with Industry, Academia, and Government) from JST, and a Grant-in-Aid for Basic Research (S) from the Ministry of Education, Culture, Sports, Science, and Technology of Japan.

[1] D. J. Müller, H. Janovjak, T. Lehto, L. Kuerschner, and K. Anderson, Prog. Biophys. Mol. Biol. **79**, 1 (2002).
[2] D. J. Müller and K. Anderson, Trends Biotechnol. **20**, S45 (2002).
[3] P. K. Hansma *et al.*, Appl. Phys. Lett. **64**, 1738 (1994).
[4] T. Ando, N. Kodera, E. Takai, D. Maruyama, K. Saito, and A. Toda, Proc. Natl. Acad. Sci. USA **98**, 12468 (2001).
[5] T. Ando, N. Kodera, D. Maruyama, E. Takai, K. Saito, and A. Toda, Jpn. J. Appl. Phys., Part 1 **41**, 4851 (2002).
[6] M. B. Viani *et al.*, Rev. Sci. Instrum. **70**, 4300 (1999).
[7] M. B. Viani *et al.*, Nat. Struct. Biol. **7**, 644 (2000).
[8] T. Sulchek, R. Hsieh, J. D. Adams, S. C. Minne, C. F. Quate, and D. M. Adderton, Rev. Sci. Instrum. **71**, 2097 (2000).
[9] B. Rogers *et al.*, Rev. Sci. Instrum. **75**, 4683 (2003).
[10] T. Sulchek, G. G. Yaralioglu, C. F. Quate, and S. C. Minne, Rev. Sci. Instrum. **73**, 2928 (2002).
[11] A. D. L. Humphris, J. K. Hobbs, and M. J. Miles, Appl. Phys. Lett. **83**, 6 (2003).
[12] M. Kitazawa, K. Shiotani, and A. Toda, Jpn. J. Appl. Phys., Part 1 **42**, 4844 (2003).
[13] N. Kodera, H. Yamashita, and T. Ando, Rev. Sci. Instrum. **76**, 053708 (2005).
[14] G. Schitter, R. W. Stark, and A. Stemmer, Ultramicroscopy **100**, 253 (2004).
[15] G. Schitter, F. Allgöwer, and A. Stemmer, Nanotechnology **15**, 108 (2004).
[16] T. Uchihashi, N. Kodera, H. Itoh, H. Yamashita, and T. Ando, Jpn. J. Appl. Phys., Part 1 **45**, 1904 (2006).
[17] T. Ando, N. Kodera, Y. Naito, T. Kinoshita, K. Furuta, and Y. Y. Toyoshima, ChemPhysChem **4**, 1196 (2003).
[18] T. Ando, T. Uchihashi, N. Kodera, A. Miyagi, R. Nakakita, H. Yamashita, and K. Matada, e-J. Surf. Sci. Nanotechnol. **3**, 384 (2005).
[19] R. D. Jäggi, A. Franco-Obregón, P. Studerus, and K. Ensslin, Appl. Phys. Lett. **79**, 135 (2001).
[20] T. R. Rodríguez and R. García, Appl. Phys. Lett. **82**, 4821 (2003).
[21] T. Ando, T. Uchihashi, N. Kodera, A. Miyagi, R. Nakakita, H. Yamashita, and M. Sakashita, Jpn. J. Appl. Phys., Part 1 **45**, 1897 (2006).
[22] R. E. Cheney, Methods Enzymol. **298**, 3 (1998).
[23] Y. Kunioka and T. Ando, J. Biochem. (Tokyo) **119**, 1024 (1996).
[24] J. H. Kindt, J. B. Thompson, M. B. Viani, and P. K. Hansma, Rev. Sci. Instrum. **73**, 2305 (2002).
[25] J. Schiener, S. Witt, M. Stark, and R. Guckenberger, Rev. Sci. Instrum. **75**, 2564 (2004).